Damage type classification based on structures nonlinear dynamical signature

Myriam Bakir, Marc Rebillat, Nazih Mechbal

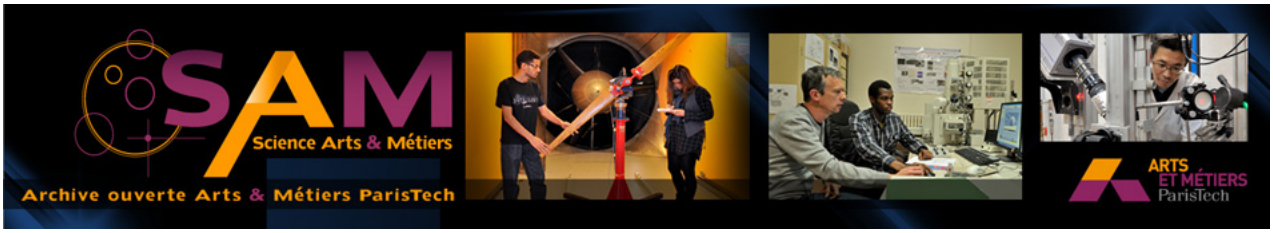

Damage type classification based on structures nonlinear dynamical signature

Myriam Bakir * **Marc Rebillat** * **Nazih Mechbal** *

* *PIMM, Arts et Métiers ParisTech, Paris, France (myriam.bakir@ensam.eu).*

Abstract: Structural damages result in nonlinear dynamical signatures that significantly help for their monitoring. A damage type classification approach is proposed here that is based on a parallel Hammerstein models representation of the structure estimated by means of the Exponential Sine Sweep Method. This estimation method has been here extended to take into account for input signal amplitude which was not the case before. On the basis of these estimated models, three amplitude dependent damage indexes are built: one that monitors the shift of the resonance frequency of the structure, another the ratio of nonlinear versus linear energy in the output signal, and a last one the ratio of the energy coming from odd nonlinearities to the energy coming from even nonlinearities in the output signal. The slopes of these amplitude-dependent DIs are then used as coordinates to place the damaged structure under study within a three-dimensional space. A single mass-spring-damper system is considered to illustrate the ability of this space to classify different types of damage. Four types of damage with different severities are simulated through different spring nonlinearities: bilinear stiffness, dead zone, saturation, and Coulomb friction. For all severities, the four types of damage are extremely well separated within the proposed three-dimensional space, thus highlighting its high potential for classification purposes.

Keywords: Structural Health Monitoring, Damage type classification, Nonlinear model estimation, Parallel Hammerstein models.

1. INTRODUCTION

The process of implementing a damage identification strategy for aeronautic or civil infrastructures is referred to as Structural Health Monitoring (SHM) and may provide considerable improvements with respect to safety and maintenance costs (Worden et al., 2007). A SHM process is classically performed in four steps: detection, localization, classification and quantification. There exists several algorithms able to handle for both the detection and localization steps, but still there is almost no reliable solution for the classification and quantification steps.

One commonly used SHM technique is that of *"active sensing"* whereby permanently attached actuators launch Lamb waves in the structure under inspection and a set of sensors records the structural responses in order to extract some damage related information (Raghavan and Cesnik, 2007). One of the outstanding advantage of using Lamb waves for SHM is that such waves can travel over relatively long distance and can be used to monitor various types of damage (such as cracks, impacts, or delaminations). Furthermore, in many cases, damages that appear on complex structures generate nonlinear dynamical responses that can be used efficiently for SHM purposes (Farrar et al., 2007; Worden et al., 2008).

Existing damage type classification procedures are based on a time representation (de Lautour and Omenzetter, 2010) or on a time-frequency representation (Chakraborty et al., 2009; Zhou et al., 2009; Das et al., 2010) of signals recorded by sensors. In those procedures a test signal is sent by an actuator and the signal received by a sensor is then modeled using various signal processing tools (matching pursuit decomposition or autoregressive models) and classified by means of various machine learning algorithms (supports vector machine, artificial neural networks or hidden Markov chains). These approaches only model the received signals at the sensor position and not the path followed by the signal from the actuator to the sensor. Furthermore they rely only on linear signal processing tools and are thus unable to take benefit of the nonlinear part of the information coming from the damage.

We thus aim here at exploiting a richer nonlinear representation of the path followed by the signal from the actuator to the sensor within the structure to develop and validate an original and simple solution for the *"classification"* step of SHM systems based on guided waves. This approach (see Fig. 1 for an overview of the procedure) is based on a Parallel Hammerstein models representation of the actuator-sensor path. Such models are classically estimated by means of Exponential Sine Sweeps put as input of the damaged nonlinear structure (Rébillat et al., 2011, 2014) but without taking into account for the input sweep amplitude. As a first contribution of the paper, this estimation method has been extended to take into account for input signal amplitude. On the basis of models estimated at different input amplitudes, three amplitude dependent damage indexes are built: the first one monitors the shift of the resonance frequency of the structure, the

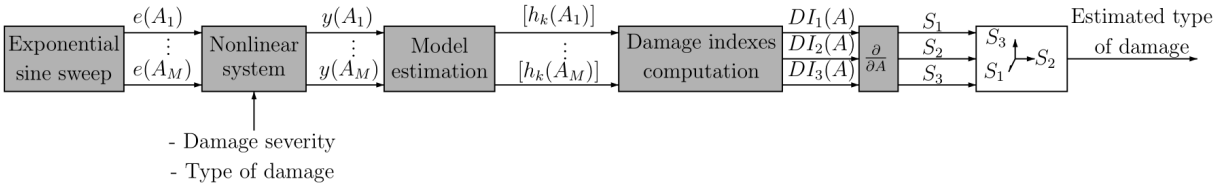

Fig. 1. Overview of the proposed classification method. Three amplitude dependent damage indexes $DI_1(A)$, $DI_2(A)$ and $DI_3(A)$ are built on the basis of nonlinear models $[h_k(A_i)]$ that are estimated at different amplitudes A_i by means of Exponential Sine Sweeps, $e(A_i)$. The slopes of these amplitude-dependent DIs, S_1, S_2, and S_3, are then used as coordinates to place the damaged structure under study within a three-dimensional space.

second the ratio of nonlinear versus linear energy in the output signal, and the last one the ratio of the energy coming from odd nonlinearities to the energy coming from even nonlinearities in the output signal. The slopes of these amplitude-dependent DIs are then used as coordinates to place the damaged structure under study within a three-dimensional space. A single mass-spring-damper system is considered to illustrate the ability of this space to classify different types of damage. Four types of damage with different severities are simulated through different spring nonlinearities: bilinear stiffness, dead zone, saturation, and Coulomb friction.

After extending the exponential sine sweep method in order to take into account for input signal amplitude (see Sec. 2), the way the amplitude-dependent damage indexes are built based on a Parallel Hammerstein models representation of the system is explained (Sec. 3). Their ability to classify several types of damage modeled as various nonlinearities is then tested numerically on a mass-spring-damper system (Sec. 4) before concluding (Sec. 5).

2. AMPLITUDE COMPENSATED PARALLEL HAMMERSTEIN MODELS ESTIMATION

2.1 Parallel Hammerstein models (PHM)

In PHM, each branch is composed of one nonlinear static polynomial element followed by a linear one $h_n(t)$ as shown in Fig. 2. The relation between the input $e(t)$ and the output $s(t)$ of such a system is given by Eq. (1) where $(*)$ denotes the convolution operator.

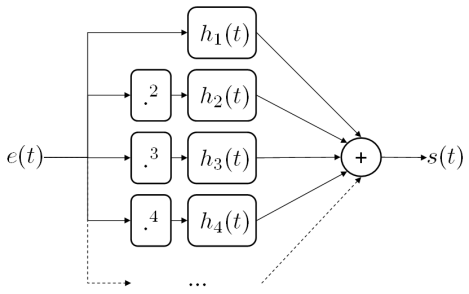

Fig. 2. Parallel Hammerstein models

$$s(t) = \sum_{n=1}^{N} \left(h_n * e^n\right)(t) \tag{1}$$

Any PHM is fully represented by its kernels $\{h_n(t)\}_{n\in\{1\dots N\}}$, which are only a set of linear filters. This model is thus interesting as it is at the same time quite simple to use and intuitive to understand.

Estimating each kernel of a PHM is not a straightforward task. As can be seen in Eq. (1), PHM are linear in the parameters to be estimated. A naive approach is to identify the model using a classical least square method. However, the least square method requires the inversion of a $MN \times MN$ matrix, where N is the order of the system under test and M is the length of the impulse responses $h_n(t)$ in samples. This matrix can be very ill-conditioned since it is generated from the exponent (until N) of the input signal. This results in important estimation errors especially in noisy conditions. Moreover the computation of the matrix from the input signal and of the inverse of the matrix is computationally costly and limits in practical case the memory M of the system. For those reasons, we rely here on an alternate estimation procedure based on exponential sine sweeps.

2.2 Exponential sine sweeps

In order to experimentally cover the frequency range over which the system under study has to be identified, cosines with time-varying frequencies and amplitude A are commonly used. When the instantaneous frequency of $e(A,t) = Acos\left[\phi(t)\right]$ is increasing exponentially from f_1 to f_2 in a time interval T, this signal is called an *"Exponential Sine Sweep"*. It can be shown (Rébillat et al., 2011) that by choosing $T = \left(2m - \frac{1}{2}\right)\frac{\ln(f_2/f_1)}{2f_1}$ with $m \in \mathbb{N}^*$, one obtains:

$$\forall k \in \mathbb{N}^* \quad cos\left[k\phi(t)\right] = cos\left[\phi(t + \Delta t_k)\right] \tag{2}$$
$$\text{with} \quad \Delta t_k = \frac{T\ln(k)}{\ln(f_2/f_1)}$$

Using Chebyshev polynomials associated to this property, $e^i(A,t)$ is rewritten as in Eq. (3).

$$e^i(A,t) = A^{i-1}\sum_{k=1}^{i} C\left(i,k\right) e\left(A, t + \Delta t_k\right) \tag{3}$$

2.3 Kernel recovery in the time domain

If an exponential sine sweep is presented at the input of PHM, by combining Eq. (1) and Eq. (2), we obtain the following relation:

$$s(A,t) = \sum_{n=1}^{N} (\gamma_n * e)(A, t + \Delta t_n) \quad (4)$$
$$\text{with} \quad \gamma_n(A,t) = A^{n-1} \sum_{k=1}^{n} c_{k,n} h_k(A,t)$$

where $\gamma_n(A,t)$ is the contribution of the different kernels to the n^{th} harmonic for an input amplitude A. In order to identify each kernel $h_n(A,t)$ separately, a signal $y(A,t)$ operating as the inverse of the input signal $e(A,t)$ in the convolution sense can be built (Rébillat et al. (2011)). After convolving the output of the PHM $s(A,t)$ given in Eq.4 with $y(A,t)$, one obtains:

$$(y * s)(A,t) = \sum_{n=1}^{N} \gamma_n(A, t + \Delta t_n) \quad (5)$$

Because $\Delta t_n \propto ln(n)$ and $f_2 > f_1$, the higher the order of non-linearity n, the more advanced the corresponding $\gamma_n(A,t)$. Thus, if T_m is chosen long enough, the different $\gamma_n(A,t)$ do not overlap in time and can be separated by simply windowing them in the time domain. Using Eq. (6), the family $\{h_n(A,t)\}_{n\in[1,N]}$ of the kernels of the PHM under study can then be fully extracted.

$$[h_1(A,t) \dots h_N(A,t)]^T = D\tilde{C}^T [\gamma_1(A,t) \dots \gamma_N(A,t)]^T$$
$$\text{with } D = diag(1, A^{-1}, \dots, A^{1-N}) \quad (6)$$

In Eq. (6), $\tilde{C^T}$ stands for the transpose of the Chebyshev matrix C from which the first column and the first row have been removed (see Rébillat et al. (2011)). The amplitude compensation term is the matrix D and constitutes an extension of previous methods (Rébillat et al., 2011).

3. NONLINEAR DAMAGE INDEXES COMPUTATION

The way the three damage indexes mentioned above are built from PHM estimated at different amplitudes A by means of the procedure described in Sec. 2 is described in this section.

3.1 PHM-based decompositions of the output signal

By rephrasing Eq. (1), it is possible to decompose the output of the PHM as follows:

$$\begin{aligned} s(A,t) &= (h_1 * e)(A,t) + \sum_{n=2}^{N} (h_n * e^n)(A,t) \\ &= s^{\text{L}}(A,t) + s^{\text{NL}}(A,t) \end{aligned} \quad (7)$$

where $s^{\text{L}}(A,t)$ stands for the linear and $s^{\text{NL}}(A,t)$ for the nonlinear parts of the output signal $s(A,t)$. It is also possible to decompose further $s^{\text{NL}}(A,t)$ in order to obtain the odd, $s_o^{\text{NL}}(A,t)$, and even, $s_e^{\text{NL}}(A,t)$, nonlinear parts of the output signal:

$$\begin{aligned} s^{\text{NL}}(A,t) &= \sum_{n \text{ odd}} (h_n * e^n)(A,t) + \sum_{n \text{ even}} (h_n * e^n)(A,t) \\ &= s_o^{\text{NL}}(A,t) + s_e^{\text{NL}}(A,t) \end{aligned} \quad (8)$$

As the input signal $e(A,t)$ is known and as the Hammerstein kernels $\{h_n(A,t)\}_{n\in[1,N]}$ have been estimated previously, those linear, and total, odd, and even nonlinear parts of the output signal are then easily evaluated thanks to the procedure described in Sec. 2 and can be used to build damage indexes. In the following sections, $S^{\text{L}}(A,f)$, $S^{\text{NL}}(A,f)$, $S_e^{\text{NL}}(A,f)$, and $S_o^{\text{NL}}(A,f)$ will be denoting the Fourier transforms of $s^{\text{L}}(A,t)$, $s^{\text{NL}}(A,t)$, $s_e^{\text{NL}}(A,t)$, and $s_o^{\text{NL}}(A,t)$.

3.2 Damage index definitions

DI_1: Classic frequency variation damage index: As a first approximation, the effect of a damage in the structure under study can be modeled as a local modification of its stiffness. Let $f_H(A)$ be the frequency of the first mode of the structure in the healthy case and $f_D(A)$ the same frequency in the damaged case for a given input amplitude A. These frequencies can here be easily extracted from the estimated nonlinear model as the kernel $h_1(A,t)$, or its Fourier transform $H_1(A,f)$, is nothing else than the linear response of the system. After the analysis of $H_1(A,f)$ in a healthy and a damaged cases, we can then define a classic linear damage index (DI) as (Salawu, 1997):

$$\text{DI}_1(A) = \frac{f_D(A) - f_H(A)}{f_H(A)} \quad (9)$$

DI_2 : Ratio of the nonlinear energy to the linear energy: Taking advantage of Eq. (7), we use a second DI that is defined as the ratio of the energy contained in the nonlinear part of the output of the PHM versus the energy contained in the linear part of the output of the PHM for a given input amplitude A (Rébillat et al., 2014). This damage index is defined as follow:

$$\text{DI}_2(A) = \frac{\int_{f_1}^{f_2} |S^{\text{NL}}(A,f)|^2 df}{\int_{f_1}^{f_2} |S^{\text{L}}(A,f)|^2 df} \quad (10)$$

where f_1 and f_2 have been defined earlier in Sec. 2.2.

DI_3 : Ratio of the even to the odd nonlinear energies: Using Eq. (8), we build a third DI that is defined as the ratio of the energy contained in the even nonlinear part of the output of the PHM versus the energy contained in its odd nonlinear part for a given input amplitude A. We build a damage index defined as follow:

$$\text{DI}_3(A) = \frac{\int_{f_1}^{f_2} |S_e^{\text{NL}}(A,f)|^2 df}{\int_{f_1}^{f_2} |S_o^{\text{NL}}(A,f)|^2 df} \quad (11)$$

4. NUMERICAL APPLICATION

4.1 Dynamical system under study

A simple spring-mass-damper system, see Fig. 3, has been chosen to demonstrate the ability of the proposed method

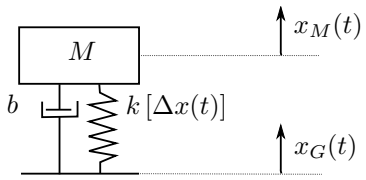

Fig. 3. Simulated spring-mass-damper system

to classify different types of damages. All the simulations are done using Simulink® and a Runge-Kutta solver. The input signal is the ground acceleration $\ddot{x}_G(t)$ and the ouptut signal is the mass acceleration $\ddot{x}_M(t)$. Both the damper and the spring are subjected to the relative displacement $\Delta x(t) = x_M(t) - x_G(t)$. For this system, the following values have been selected: $M = 450$ kg, $b = 10^3$ Ns/m, and $k = 10^6$ N/m. The mechanical equation of this kind of system is then:

$$M\ddot{x}_M(t) = -F\left[\Delta x(t)\right] - b\Delta\dot{x}(t) \tag{12}$$

where $F\left[\Delta x(t)\right]$ is the force associated with the spring, and is assumed to be linear and given by $F\left[\Delta x(t)\right] = k\Delta x(t)$ in the healthy state of the system.

At the end of the simulation, some noise (Gaussian noise of zero mean and scaled variance) is added to the output signal. The signal to noise ratio (SNR) is defined here as the ratio in dB between the maximum amplitude of the output acceleration in the linear healthy case ($k \times x_{lim}/M$) to the standard deviation of the added noise. x_{lim} denotes the maximum relative displacement in the linear case.

4.2 Considered damage types

Four types of damage with different severities are simulated through different spring nonlinearities: bilinear stiffness, dead zone, saturation, and Coulomb friction. By denoting $\alpha \in [0, 1]$ the damage severity coefficient ($\alpha = 0$: healthy, and $\alpha = 1$: totally damaged) the restoring forces $F\left[\Delta x(t)\right]$ associated with the different nonlinear damages are expressed as in Tab. 1. To calibrate the nonlinearities, two additional parameters are needed, x_{lim} and x_{low}. The former is defined as the maximum relative displacement in the linear case while the latter corresponds to the static relative displacement in the linear case.

The four nonlinearities have been chosen as idealized representations of four types of damages:

- The *bilinear stiffness* corresponds to a crack that is opening and closing and thus that presents different stiffnesses depending on its state. For the bilinear stiffness the severity parameter α corresponds to the relative stiffness decrease when the crack opens.
- The *saturation* can be seen as a dry friction phenomenon associated with a spring and may correspond to relative movements between parts of a system caused by an overdrive in force. The severity α has been defined as a system that never saturates when $\alpha = 0$ and that always saturate when $\alpha = 1$. Furthermore α has been scaled not to grow too quickly (see Tab. 1).
- The *dead zone* models systems where damage causes some mechanical slack without any contact between two parts. The severity α has been defined as a system without any slack when $\alpha = 0$ and with a slack of $10\% \times x_{low}$ when $\alpha = 1$.
- The *Coulomb friction* models systems where damage manifests itself by the appearance of Coulomb friction due for example to the lack of lubrification between parts. The severity α has been defined as a system without any Coulomb friction when $\alpha = 0$ and with a Coulomb force of $10\% \times k \times x_{low}$ when $\alpha = 1$.

Bilinear stiffness
$F\left[\Delta x(t)\right] = \begin{cases} k\Delta x & \text{if } \Delta x < 0 \\ (1-\alpha_l)k\Delta x & \text{if } \Delta x \geq 0 \end{cases}$
$\alpha_l = \alpha$
Saturation
$F\left[\Delta x(t)\right] = \begin{cases} k\Delta x & \text{if } \lvert\Delta x\rvert < \alpha_s x_{lim} \\ k\alpha_s x_{lim} & \text{else} \end{cases}$
$\alpha_s = (1 - (log_2(1+\alpha))^{\frac{1}{4}})$
Dead zone
$F\left[\Delta x(t)\right] = \begin{cases} k\Delta x + k\alpha_d x_{low} & \text{if } \Delta x < -\alpha_d x_{low} \\ k\Delta x - k\alpha_d x_{low} & \text{if } \Delta x \geq \alpha_d x_{low} \\ 0 & \text{else} \end{cases}$
$\alpha_c = 0.1\alpha$
Coulomb friction
$F\left[\Delta x(t)\right] = \begin{cases} k(\Delta x - \alpha_c x_{low}) & \text{if } \Delta x < 0 \\ k(\Delta x + \alpha_c x_{low}) & \text{if } \Delta x \geq 0 \end{cases}$
$\alpha_c = 0.1\alpha$

Table 1. Nonlinear considered damage types.

4.3 Amplitude-compensated PHM

For bilinear damage type and severity $\alpha = 0.6$ (see Sec. 4.2), the first step consists in the generation of the exponential sine sweep input signals for different given amplitudes as shown in Fig. 4(a). We chose $f_1 = 0.7$ Hz and $f_2 = 25$ Hz to cover a range of frequencies that includes the linear resonance that is around 7 Hz here and can be observed in the output signal in Fig. 4(a). The duration of the signal is fixed at $T = 150/f_1$, the order of the Hammerstein estimation at $N = 4$ and the sampling frequency is defined by $f_s = 2f_2N\omega$, where ω is a safety coefficient set to 1.1. The estimated PHM representation of the damaged structure is shown in Fig. 4(b). On the first kernel we recognize the typical response of a linear resonant system and we can see that outside the excited frequency range, the system is not characterized. As expected, the increase of the input amplitude causes the growth of harmonics that can be seen on the kernels of orders 2, 3, and 4.

4.4 Damage index computation

The kernels are then used to compute the three DIs $DI_1(A)$, $DI_2(A)$, and $DI_3(A)$ (as shown in Fig. 5 for the different type of damages and for different damage severities) and their mean slopes S_1, S_2, and S_3. Fig. 5 shows that the global behavior of the DIs depends mainly on the chosen type of damage, and not on its severity if it is high enough (*i.e.* for $\alpha > 10 - 15\%$ here). Furthermore, by comparing each type of damage to the others, one can see that the magnitude of the variation of the DIs is representative of the type of damage.

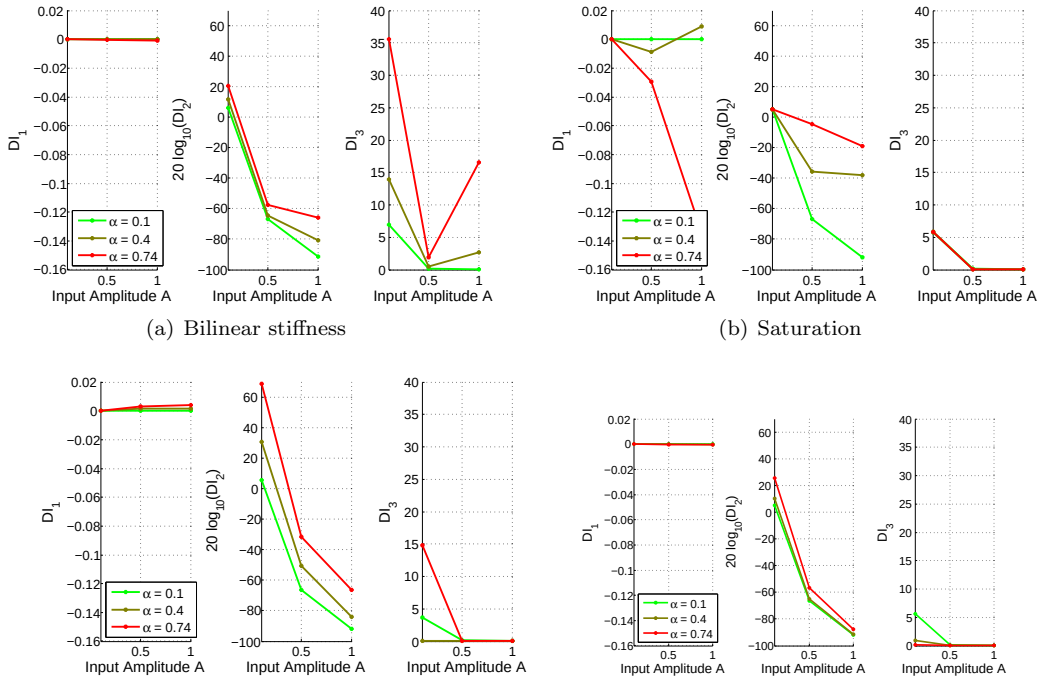

(a) Bilinear stiffness (b) Saturation

(c) Dead zone (d) Coulomb friction

Fig. 5. Damage indexes evolution with input amplitude for several severities for the different types of nonlinear damages.

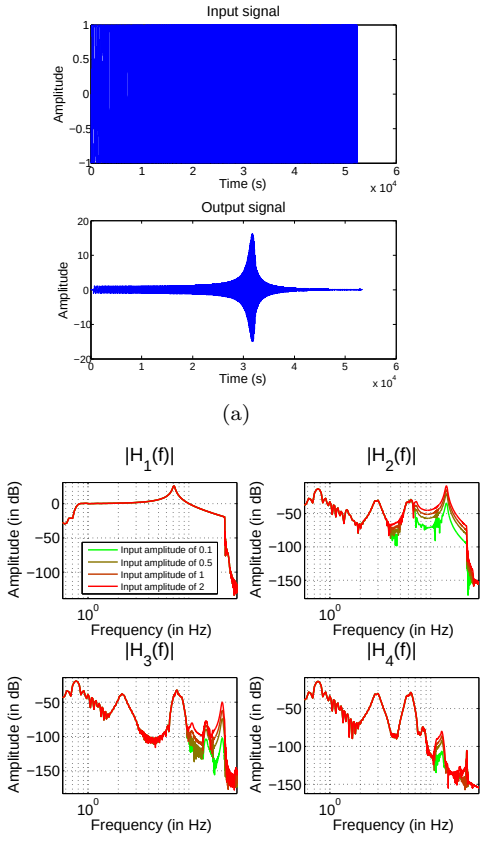

(a)

(b)

Fig. 4. (a) Input (top) and output (bottom) signals for a bilinear spring at $\alpha = 0.6$ and an amplitude of 1. (b) Estimation of the 4 first kernels for a bilinear spring at $\alpha = 0.6$.

4.5 Proposed classification space

In Fig. 6(a), each point representing one type of damage with one severity level, is placed in the (S_1, S_2, S_3) space. As it can easily be seen, the four damage types are well separated in this space, thus assessing the efficiency of the proposed space for classification purposes. As can be seen, when the SNR is 120 dB, see Fig. 6(a), the classification space is almost not affected by noise. When decreasing the SNR to 100 dB, see Fig. 6(b), the classification space is more affected and specially the points associated with the saturated spring. However, for this SNR, the global organisation of the space is still intact.

5. DISCUSSION AND CONCLUSION

A nonlinear damage type classification approach is proposed here that is based on a PHM representation of the structure. Such models are estimated at different amplitudes by means of an adapted version of the Exponential Sine Sweep Method. On the basis of these estimated models, three amplitude dependent damage indexes are built. The slope of these amplitude-dependent DIs are then used as coordinates to place the damaged structure under study within a three-dimensional space. A single mass-spring-damper system is considered to highlight the ability of this space to classify different types of damage.

However, one can still not conclude regarding the general validity of such a classification space and the results presented here only constitute preliminary work. Indeed, this space has for the moment not been used in conjunction with any machine learning algorithm (such as support vector machine for example). Furthermore, the chosen numerical example is very simple and not representative of real life complex structures. A beam simulated by means

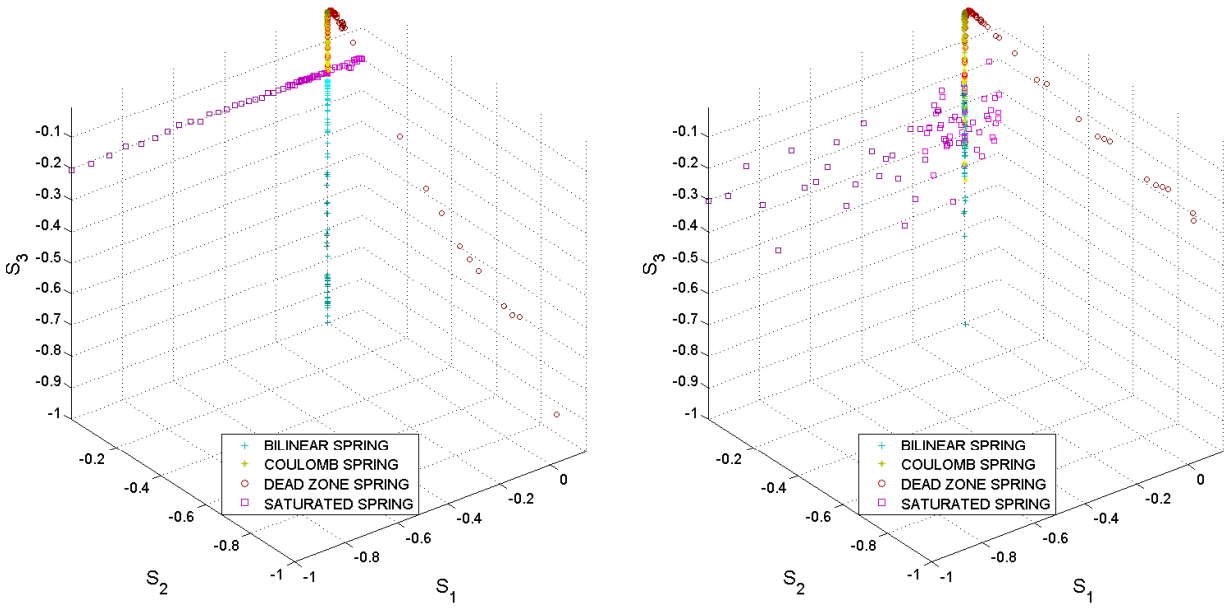

(a) SNR= 120 (b) SNR= 100

Fig. 6. Evolution of the mean slopes of the damage indexes for several damage severities, for the different types of considered nonlinear damages, and for different SNRs.

of a finite-element model on which a nonlinear damage is inserted at a given node could for example be considered.

ACKNOWLEDGEMENTS

This work has been founded partially by the CORALIE project: CORAC/EPICE-AP2-P6-07/CORALIE.

REFERENCES

Chakraborty, D., Kovvali, N., Wei, J., Papandreou-Suppappola, A., Cochran, D., and Chattopadhyay, A. (2009). Damage classification structural health monitoring in bolted structures using time-frequency techniques. *Journal of Intelligent Material Systems and Structures*, 20(11), 1289–1305.

Das, S., Chattopadhyay, A., and Srivastava, A.N. (2010). Classifying induced damage in composite plates using one-class support vector machines. *Aiaa Journal*, 48(4), 705–718.

de Lautour, O.R. and Omenzetter, P. (2010). Damage classification and estimation in experimental structures using time series analysis and pattern recognition. *Mechanical Systems and Signal Processing*, 24(5), 1556–1569.

Farrar, C.R., Worden, K., Todd, M.D., Park, G., Nichols, J., Adams, D.E., Bement, M.T., and Farinholt, M.T. (2007). Nonlinear system identification for damage detection. Technical report, Los Alamos National Laboratory.

Raghavan, A. and Cesnik, C.E.S. (2007). Review of guided-wave structural health monitoring. *The Shock and Vibration Digest*, 39(91).

Rébillat, M., Hajrya, R., and Mechbal, N. (2014). Nonlinear structural damage detection based on cascade of hammerstein models. *Mechanical Systems and Signal Processing*, 48(1-2), 247–259.

Rébillat, M., Hennequin, R., Corteel, E., and Katz, B.F.G. (2011). Identification of cascade of Hammerstein models for the description of nonlinearities in vibrating devices. *Journal of Sound and Vibration*, 330(5), 1018–1038.

Salawu, O. (1997). Detection of structural damage through changes in frequency: a review. *Engineering Structures*, 19(9), 718 – 723.

Worden, K., Farrar, C.R., Haywood, J., and Todd, M. (2008). A review of nonlinear dynamics applications to structural health monitoring. *Structural Control & Health Monitoring*, 15(4), 540–567.

Worden, K., Farrar, C.R., Manson, G., and Park, G. (2007). The fundamental axioms of structural health monitoring. *Proceedings of the Royal Society A: Mathematical, Physical and Engineering Science*, 463(2082), 1639–1664.

Zhou, W.F., Kovvali, N., Reynolds, W., Papandreou-Suppappola, A., Chattopadhyay, A., and Cochran, D. (2009). On the use of hidden markov modeling and time-frequency features for damage classification in composite structures. *Journal of Intelligent Material Systems and Structures*, 20(11), 1271–1288.